FABRICATION AND PROFILING OF TiO_2 THIN FILMS VIA LOW-TEMPERATURE SYNTHESIS

Nyo Mar Soe[1], Soe Ko Ko Aung[2] and Yin Maung Maung[3]

Abstract

The focus on low-temperature processed electron transport layers (ETLs) has gained significant attention for the fabrication of flexible perovskite solar cells. In this study, anatase titanium dioxide (TiO_2) nanoparticles were synthesized via a hydrothermal method and applied using the spin-coating technique, with annealing performed at 200 °C. X-ray diffraction analysis confirmed the crystal structures of the TiO_2 film. Additionally, the UV-Vis spectrum revealed a high transmittance exceeding 80%. The energy band gap (3.25 eV) and thickness (542 nm) of the TiO_2 film were determined through Tauc's plot method and Envelope method, respectively. These findings suggest that this straightforward approach to preparing TiO_2 ETLs holds promise for integration into the fabrication of perovskite solar cells.

Keywords*:* Titanium dioxide (TiO_2), Electron Transport Layer (ETL), Spin coating method, Optical properties

Introduction

Solar cells have supplied a solution to the energy crisis and environmental contamination because of their potential to use solar energy (F. Rehman et al., 2023). Solar cells (SCs) can overcome the energy crisis for environmental all over the world. The fabrication of solar cell is completed with a suitable band energy alignment at the interface of two layers through unlike semiconductors. In addition, absorption of light, charge charriers, restriction of recombination loss and quality of selected material support solar cell system (H. Soonmin et al., 2023). First generation solar cells were fundamentals silicon p-n junction semiconductor. Second generation solar cells based on are thin-film technologies, especially based on amorphous silicon (a-Si) and inorganic substances such as copper indium gallium selenide (CIGS) and cadmium telluride (CdTe) with a larger absorption coefficient (B. P. Singh et al., 2021). Third-generation solar cells are dye-sensitized solar cells (DSSCs), perovskite solar cells (PSC), and quantum dot sensitized solar cells (QDSSCs) are being widely discovered and undergoing rapidly development. Their implementation with thin-film technologies could have an enormous impact economical friendly, making solar energy one of the most available and cheapest selection for future energy production (N. Shah et al., 2023).

To date, perovskite solar cells (PSCs) have been enhanced power conversion efficiency (PCE) from 3.8% to 26.1% in 2024. Perovskite Solar Cells will be built electron transport layer (ETL), hole transport layer (HTL), perovskite layer and metal electrode. Among them, electron transport layer is crucial to overcome band alignment issues and improve electron transport. Moreover, ETLs are basically used to increase device performance and stability of perovskite solar cells. Metal oxide semiconductors involved titanium dioxide, zinc oxide, tin oxide, etc. Low temperature processed semiconductor metal oxides, such as cadmium selenide (CdSe), zinc oxide (ZnO) and ternary metal oxides have been explored as a potential contender to replace TiO_2 since TiO_2 must be post-treated at high temperature (Z. Yin, et al., 2022). These devices achieve high power conversion efficiencies (15−22%) but mainly require high-temperature sintering (>450 °C), which is not possible for temperature-sensitive substrates. To overcome these issues, alternative low-temperature (<150 °C) processed carbon-based PSCs will be fabricated to realize high-efficiency TiO_2based efficient perovskite solar cells. Low temperature processed carbon-based perovskite cells (C-PSCs) have gained great attention because of ease of fabrication and

[1] Department of Physics, Yangon University of Distance Education
[2] Department of Physics, University of Mandalay
[3] Department of Physics, University of Yangon

low cost (S. K. K. Aung, et al., 2022). In addition, hydrothermal synthesis method of TiO_2 benefits the ability to create crystalline phase and do not require high temperature calcination (H. G. Hameed et al., 2023). It is less energy consumption and also cost effectiveness.

The present work purposes to identify the crystal structure and the optical properties of anatase TiO_2 films. In addition, energy band gap and thickness of prepared film are calculated by Tauc's plot method and envelope method. The results show that high transmission (above 80%) TiO_2 film at 200 °C which is a suitable electron transport layer in low temperature processed fabrication in perovskite solar cells.

Materials and Methods

Preparation of TiO_2 Thin Film

Firstly, fluorine-doped tin oxide (FTO) pure glass substrates of 1cm × 1cm were created and cleaned with a small amount of detergent and water followed by acetone, ethanol and isopropanol in ultrasonic vibration for 15 mins to remove impurities. After that, the substrates were dried with dryer. Then, 23 ml of acetic acid and 100 ml of distilled water (DW) were combined to get 4 M of acetic acid solution. At the same time, 30 ml of titanium tetraisopropoxide (TTIP) and 100 ml of DW were also mixed to get 1M of titanium tetraisopropoxide solution. Subsequently, 20 ml of acetic acid solution was combined with 100 ml of TTIP solution and the mixture solution was stirred for 1 h. After stirring, the mixture was kept for 24-hours at room temperature. After 24-hours, the mixture was transferred to a Teflon-lined autoclave and dried at 180 °C for 6h in a muffle furnace. And then, the autoclave was cooled down to room temperature. The colloidal solution was coated onto a silicon wafer by using spin coating technique. The structured properties of TiO_2 coated Si wafer were examined by XRD analysis. Furthermore, 200µL of colloidal solution was dropped on the FTO cleaned substrate via 100 µL-1000 µL pipette and spin coated with 3000 rpm for 30 s. Then resultant substrates were annealed at 200 °C on the hot plate for 30 mins. In order to know the optical properties of TiO_2 coated FTO thin film, UV-vis spectroscopy was employed. The schematic diagram of the synthesis of the TiO_2 thin film was shown in Figure 1 and the photograph of the synthesis of TiO_2 thin film was also shown in Figure 2.

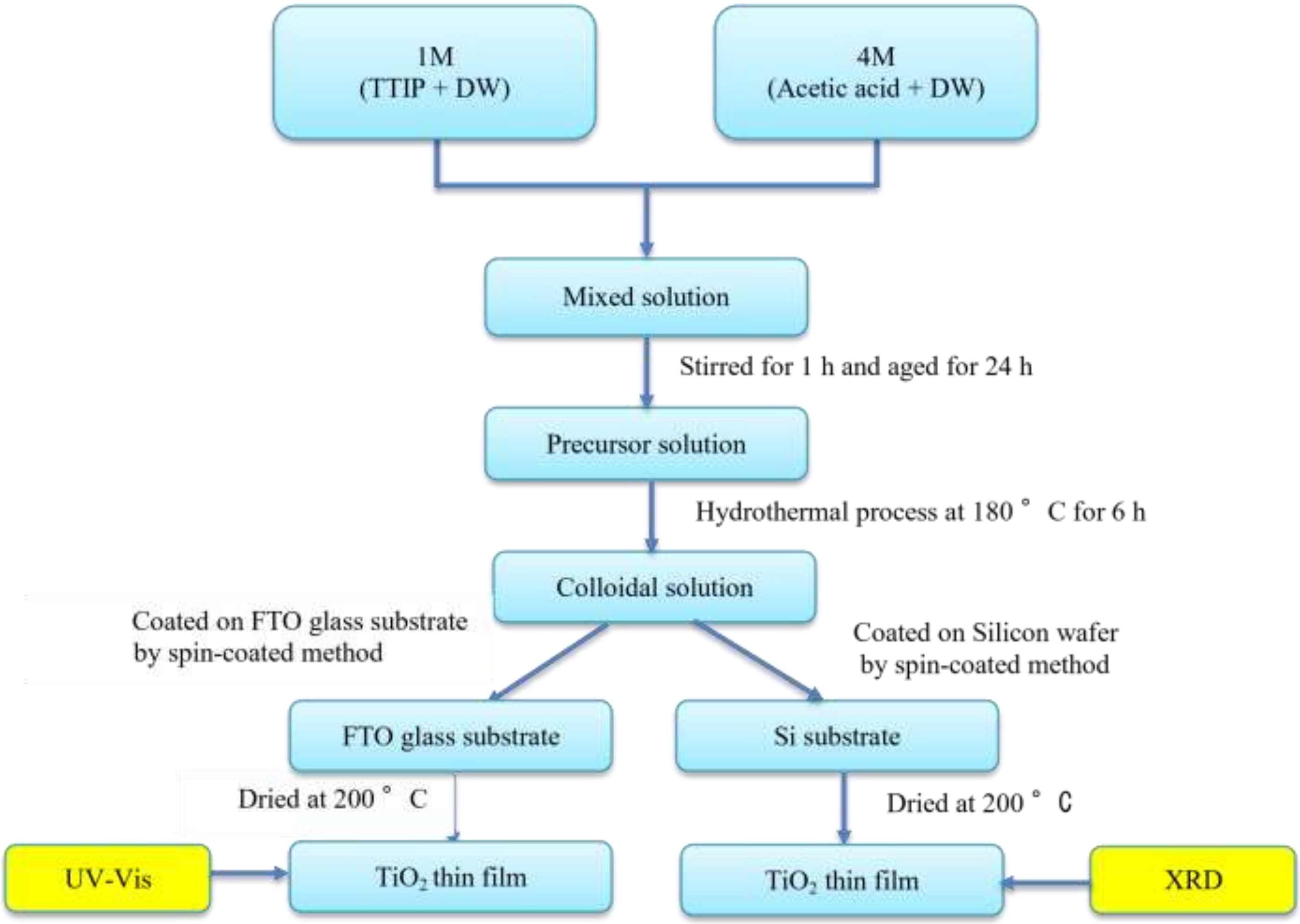

Figure. 1 Schematic diagram of the synthesis of TiO_2 thin film

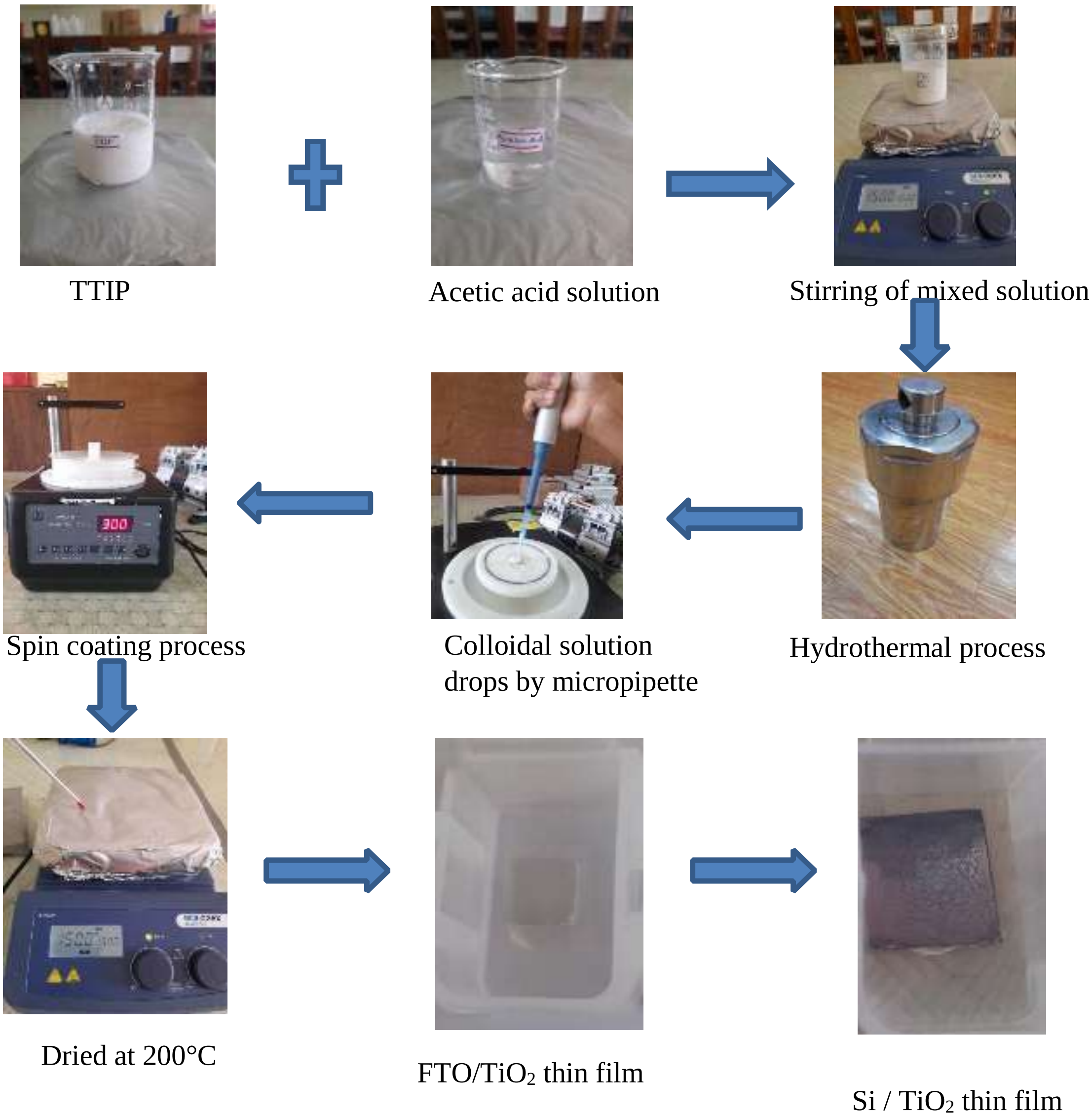

Figure. 2 Photograph of the synthesis of TiO_2 thin film

Characterization techniques

The optical properties of TiO_2 thin film were recorded in the wavelength range between 190 – 1100 nm by using UV-Vis spectrophotometer (Thermo Genesys 10S). The crystal structure of prepared films was measured using SmartLab Rigaku.

Results and Discussion

XRD Analysis of TiO2 Thin Film

The crystal structures of TiO_2 thin film were confirmed by X-ray diffraction (XRD) spectra using Cu-Kα radiation (1.54059 Å) at a scanning range of 10−60° (Rigaku Corporation) seen in Figure 3. The characteristic peaks corresponded well with the JCPDS card (21–1272), inferring an anatase type of TiO_2 was formed. The XRD spectrum revealed prominent diffraction peaks at 24.72° (101), 37.27° (004), 47.43° (200), 53.51° (105), and 54.59° (211), aligning with the anatase phase of TiO_2. Furthermore, the average crystallite size was determined by the Debye-Scherrer equation using the following equation: $D = K\lambda/\beta\cos\theta$, where, λ= wavelength of the incident X-ray beam (1.5405 Å) for CuKα, K = shape factor constant, β = FWHM (full width at half maximum) (radian), θ = diffraction angle (radian) and D = crystallite size (nm) (T.

Theivasanthi, et al., 2023). The average crystallite size of the TiO_2 particle was to be approximately 16.89 nm listed in Table 1.

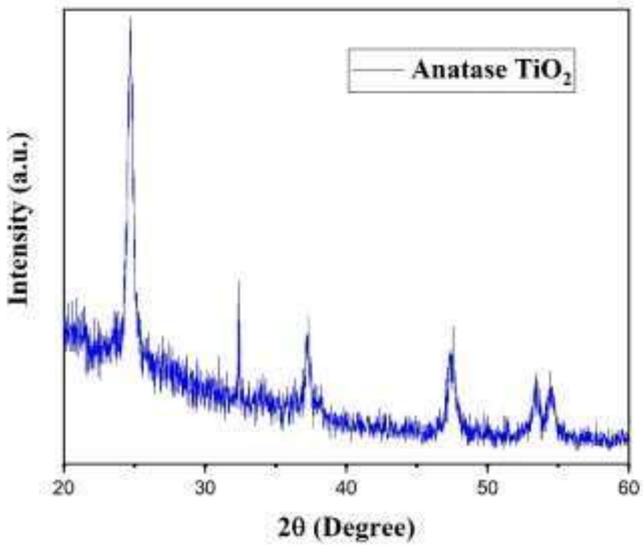

Figure. 3 XRD pattern of TiO_2 thin film

Table 1. Crystallites (grain) size from XRD data using Debye-Scherrer equation.

No.	**2θ (degree)**	**FWHM (degree)**	**(hkl)**	**Crystallite size (D) (nm)**
1	24.72	0.47	(101)	17.1177
2	37.27	0.39	(004)	21.2792
3	47.43	0.66	(200)	12.9999
4	53.51	0.53	(105)	16.5109
5	54.59	1.53	(211)	16.5905
Average crystallite size				**16.89 nm**

Optical Properties of TiO_2 Thin Film

The UV-Vis spectrum describes that how much a sample component absorption light in the thin film area due to it is scanned through each wavelength in the ultraviolet-visible range of the electromagnetic radiation. The transmission and absorption spectra emerge at each wavelength. Figure 4 showed UV-Vis transmission spectra of TiO_2 coated FTO substrate and bare FTO substrate in the wavelength range 300-900 nm. Transmittance data for FTO /TiO_2 and FTO films were listed in Table 2. It was found that the transmittance spectrum of the TiO_2 coated FTO substrate which is slightly lower than that of the bare FTO substrate.

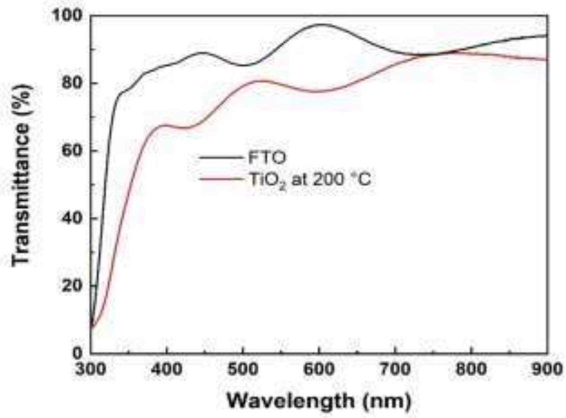

Figure. 4 UV-Vis transmission spectra of TiO_2 thin film

Table 2. Transmittance (%) data for TiO_2 thin film and FTO

Film	Wavelength (nm)			Transmittance (%)		
	1st peak	2nd peak	3rd peak	1st peak	2nd peak	3rd peak
FTO	336	446	601	76	89	**97**
TiO_2	395	520	774	67	81	**89**

Optical Band Gap Calculation

The band gap shows a specific minimum energy for an electron to jump from the valence band to the conduction band (K. M. Reddy, et al., 2003). Optical band energy was determined from the absorption spectrum by applying Tauc's plot equation:$(\alpha h \nu)^n = A (h \nu E_g)$ where, E_g is the optical band gap and α is the absorption coefficient. The optical energy gap of TiO_2 was observed for indirect transition (n=1/2) and the optical energy gap of FTO was examined for direct transition (n= 2). Then, the plot of deviation of $(\alpha h \nu)^{1/2}$ for TiO_2 and $(\alpha h \nu)^2$ were demonstrated in Figure 5. The calculated energy gap for TiO_2 (3.25 eV) was lower than that of FTO (3.75 eV) due to decreased in transmittance corresponding to increase in thickness. Hence, we investigated the thicknesses of FTO/TiO_2 and FTO substrates by using Swanepoel's envelope method. Energy band gap data for FTO/TiO_2 and FTO films were listed in Table 3.

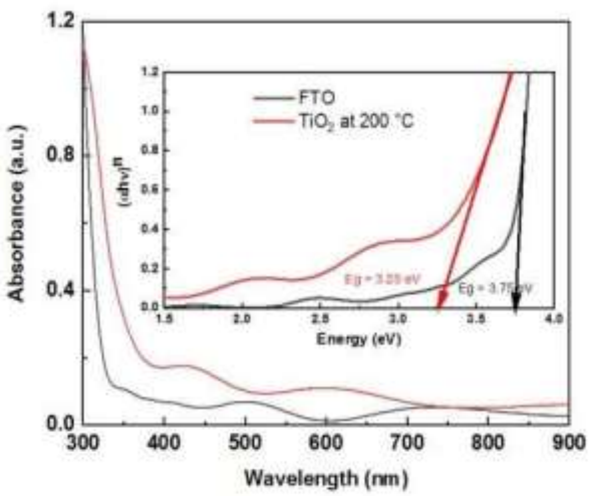

Figure. 5 UV-Vis absorption spectra of TiO_2 thin film

Table 3. Energy band gap data for TiO_2 thin film and FTO

Film	Energy Band Gap (eV)	Thickness (nm)
TiO_2	3.25	542
FTO	3.75	604

Determination of thin film thickness

When the light interference from the two surface of thin film, transmission spectrum of thin film can be observed in the spectral regions of weak and medium absorption. Thickness of TiO_2 thin film can be examined from the interference peaks of the transmission spectrum over the visible region. The estimation of refractive index, n of thin film in weak and medium absorption at each wavelength can be calculated by using upper envelope of the curve, T_M and lower envelope of the curve, T_m in the transmission spectrum, $n = [\, N + (N^2 - s^2)^{1/2} \,]^{1/2}$ where, $N = 2s\,(\frac{T_M - T_m}{T_M T_m}) + \frac{s^2+1}{2}$, s is the refractive index of the substrate (E. R. Shaaban, et al., 2012). n_1 and n_2 are refractive indices for two adjacent maxima or minima at the wavelengths of λ_1 and λ_2 as well as λ_2 and λ_1. Finally, thickness of films from the transmission spectra can be calculated using the following equation, $d = \frac{\lambda_1 \lambda_2}{2(\lambda_1 n_2 - \lambda_2 n_1)}$. The thickness of TiO_2 thin film (542 nm) was lower than that of FTO film (604) can be seen in Figure 6(a) and (b) determined by envelop method. In these figures, the envelopes pass through tangentially through transmission curve in the range 300-900 nm. The interference fringes were observed in the transmittance spectra for TiO_2 film as deposited on FTO glass substrate annealed at 200°C. This result showed that the roughness is related to the surface fluctuations. The calculated refractive index and thickness values were given in Table 4.

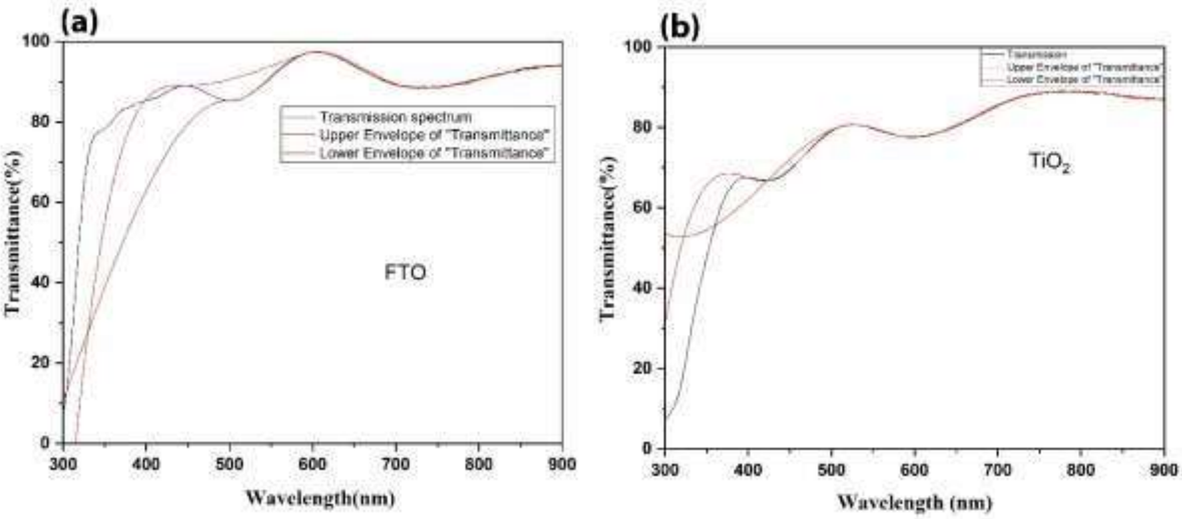

Figure 6. Thicknesses determination of (a) FTO film and (b) TiO_2 film

Table 4. Thickness data for FTO and TiO_2 films

Film	λ_1 (nm)	λ_2 (nm)	Refractive index (n_1)	Refractive index (n_2)	Thickness (d) (nm)
FTO	584	444	1.5101	1.5156	604
TiO_2	507	389	1.5099	1.5168	542

Conclusions

In this study, anatase TiO_2 nanoparticles were synthesized through a hydrothermal route and applied them using the spin-coating method, with annealing performed at 200 °C. The XRD results indicated well-defined characteristic peaks of TiO_2, confirming the formation of an anatase type. The TiO_2 thin film exhibited excellent transmission exceeding 80%, and the UV-Vis spectra revealed an optical bandgap of 3.25 eV. Utilizing Swanepoel's envelope method, we determined the thickness of the TiO_2 film to be 542 nm. This research establishes that the TiO_2 thin film, processed at 200°C, is well-suited as an electron transport layer in perovskite solar cells.

Acknowledgements

I especially thank you to Prof Dr Khin Khin Kyaw, Head of Department of Physics, Yangon University of Distance Education, for her kind permission to contribute of this work. My special thanks go to Prof Dr Hsun Lwin, Department of Physics, Yangon University of Distance Education, for his permission to contribute of this work. I sincerely thank to Prof Dr Cho Cho Thet, Department of Physics, University of Yangon, for giving encouragement of this work. Author thanks to international science programme (ISP), Uppsala University for providing research facilities.

References

B. P. Singh, S. K. Goyal, and P. Kumar, (2021) "Solar pv cell materials and technologies: Analyzing the recent developments," *Mater. Today Proc.*, vol. 43, pp. 2843–2849, doi: 10.1016/j.matpr.2021.01.003.

E.R. Shaaban, I. S. Yahia, and E. G. El-Metwally, (2012) "Validity of swanepoel's method for calculating the optical constants of thick films," *Acta Phys. Pol. A*, vol. 121, no. 3, pp. 628–635, doi: 10.12693/APhysPolA.121.628.

E. Rehman *et al.*, (2023) "Fourth-generation solar cells: a review," *Energy Adv.*, vol. 2, no. 9, pp. 1239–1262, doi: 10.1039/d3ya00179b.

H. G. Hameed and N. A. Abdulrahman, (2023) "Synthesis of TiO2 Nanoparticles by Hydrothermal Method and Characterization of their Antibacterial Activity: Investigation of the Impact of Magnetism on the Photocatalytic Properties of the Nanoparticles," *Phys. Chem. Res.*, vol. 11, no. 4, pp. 771–782, doi: 10.22036/pcr.2022.351688.2137.

H. Soonmin, Hardani, P. Nandi, B. S. Mwankemwa, T. D. Malevu, and M. I. Malik, (2023) "Overview on Different Types of Solar Cells: An Update," *Appl. Sci.*, vol. 13, no. 4, pp. 1–37, doi: 10.3390/app13042051.

K. M. Reddy, S. V. Manorama, and A. R. Reddy, (2003) "Bandgap studies on anatase titanium dioxide nanoparticles," *Mater. Chem. Phys.*, vol. 78, no. 1, pp. 239–245, doi: 10.1016/S0254-0584(02)00343-7.

N. Shah *et al.*, (2023) "A Review of Third Generation Solar Cells," *Processes*, vol. 11, no. 6, doi: 10.3390/pr11061852.

S. K. K. Aung, A. Vijayan, M. Karimipour, T. Seetawan, and G. Boschloo, (2023) "Reduced hysteresis and enhanced air stability of low-temperature processed carbon-based perovskite solar cells by surface modification," *Electrochim. Acta*, vol. 443, p. 141935 doi: 10.1016/j.electacta.2023.141935.

S. Theivasanthi and M. Alagar, (2013) "Titanium dioxide (TiO2) Nanoparticles XRD Analyses: An Insight," 2013, [Online]. Available: http://arxiv.org/abs/1307.1091

Z. Yin, B. Lu, Y. Chen, and C. Guo, (2022) "Advances of Commercial and Biological Materials for Electron Transport Layers in Biological Applications," *Front. Bioeng. Biotechnol.*, vol. 10, no. May, pp. 1–20, 2022, doi: 10.3389/fbioe.2022.900269.